AIP | Journal of Applied Physics

Electroosmotic transport in polyelectrolyte-grafted nanochannels with pH-dependent charge density

Guang Chen and Siddhartha Das

Citation: Journal of Applied Physics **117**, 185304 (2015); doi: 10.1063/1.4919813
View online: http://dx.doi.org/10.1063/1.4919813
View Table of Contents: http://scitation.aip.org/content/aip/journal/jap/117/18?ver=pdfcov
Published by the AIP Publishing

Electroosmotic transport in polyelectrolyte-grafted nanochannels with pH-dependent charge density

Guang Chen and Siddhartha Das[a)]
Department of Mechanical Engineering, University of Maryland, College Park, Maryland 20742, USA

(Received 27 January 2015; accepted 24 April 2015; published online 11 May 2015)

"Smart" polyelectrolyte-grafted or "soft" nanochannels with pH-responsiveness have shown great promise for applications like manipulation of ion transport, ion sensing and selection, current rectification, and many more. In this paper, we develop a theory to study the electroosmotic transport in a polyelectrolyte-grafted (or soft) nanochannel with pH-dependent charge density. In one of our recent studies, we have identified that explicit consideration of hydrogen ion concentration is mandatory for appropriately describing the electrostatics of such systems and the resulting monomer concentration must obey a *non-unique*, *cubic* distribution. Here, we use this electrostatic calculation to study the corresponding electroosmotic transport. We establish that the effect of pH in the electroosmotic transport in polyelectrolyte-grafted nanochannels introduces two separate issues: first is the consideration of the hydrogen and hydroxyl ion concentrations in describing the electroosmotic body force, and second is the consideration of the appropriate drag force that bears the signature of this cubic monomeric distribution. Our results indicate that the strength of the electroosmotic velocity for the pH-dependent case is always smaller than that for the pH-independent case, with the extent of this difference being a function of the system parameters. Such nature of the electroosmotic transport will be extremely significant in suppressing the electroosmotic flow strength with implications in large number applications such as capillary electrophoresis induced separation, electric field mediated DNA elongation, electrophoretic DNA nanopore sequencing, and many more. © *2015 AIP Publishing LLC*. [http://dx.doi.org/10.1063/1.4919813]

I. INTRODUCTION

Nanochannels with grafted polyelectrolytes, often denoted as *soft nanochannels*, have been used for a variety of applications such as manipulation and switching of ion transport,[1,2] ion retification,[3] chemical sensing,[4] flow control,[5] developing devices for energy applications,[6,7] characterizing gels and elastomers,[8] and many more. These polyelectrolytes are end-grafted and hence are in a *brush-like* conformation,[9,10] and their presence makes the nanochannels "smart" and stimuli-responsive, endowing them with remarkable flexibilities that aid in the above-stated applications.

The modeling effort of ion and liquid transport in soft nanochannels can primarily be divided into two parts. The first part focuses on establishing the combined equilibrium picture of the conformation of the polyelectrolyte brushes and the electric double layer (or EDL) ion distribution. The second part concentrates in using this equilibrium calculation to quantify issues such as ion transport, electroosmotic transport in soft nanochannels, and electrophoretic mobility of soft charged particles. For the first part, both continuum as well as molecular simulation techniques have been employed. The continuum models, based on approaches such as *Self Consistent Field Theory*,[11–16] *Mean Field Lattice Theory*,[17] and *Density Functional Theory*,[18] have predicted the manner in which the equilibrium polyelectrolyte layer (PEL) structure can be regulated by adjusting the salt concentration and the pH of the electrolyte that is in contact with the PEL. The molecular scale simulations, on the other hand, have provided validation of the results obtained from the self consistent field theory[19] and unraveled aspects such as difference in dynamics between single chain and bundles of chain,[20] interaction between bottle-brush polyelectrolytes,[21] dynamics of planar polyelectrolytes in poor solvent,[22] response of polyelectrolyte brushes in the presence of external electric field[23,24] and solvent of different quality,[25] and many more. Despite such progress, there still remain several outstanding issues. One such issue is that this combined equilibrium modeling has often disregarded the effect of consideration explicit hydrogen ion concentration for cases where the PEL charge density is pH dependent. In a recent study,[26] we demonstrated the overwhelming effect of such a consideration of explicit hydrogen ion concentration. We employed a rigorous free energy model to demonstrate that such explicit consideration of hydrogen ion concentration is mandatory for describing the electrostatics of PEL with pH-dependent charge density. More importantly, such a consideration enforces the monomer distribution within the PEL to be non-uniform and to obey a *non-unique cubic profile*. It is worthwhile to mention here another study,[27] where we studied the influence of variation in pH in affecting the electrostatics of a soft spherical particle with a charged core. This study is of great relevance to interpret the electrokinetic properties of biological moieties like MS2 bacteriophage virus.

Similar to the first part, for the second part too, both continuum and atomistic simulations have been employed for the modeling purposes. For example, continuum approaches, such as Navier-Stokes equations, have been employed to obtain the soft nanochannel electroosmotic

a)E-mail: sidd@umd.edu

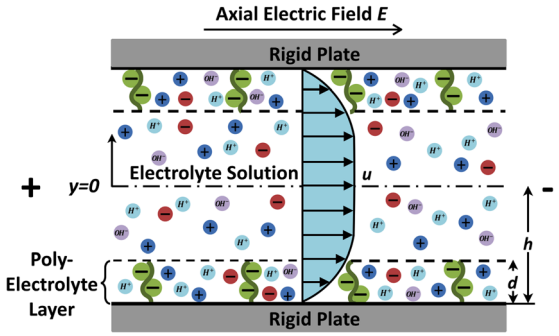

FIG. 1. Schematic of the electroosmotic flow profile in a polyelectrolyte-grafted nanochannel. The PEL ions are shown in green.

velocity field,[6,8,28] whereas a perturbation-based method has been employed for calculating the electrophoretic mobility of soft charged particles.[29–32] Similarly several atomistic models have been proposed attempting to capture different issues of electrokinetics of soft charged interfaces and soft nanochannels.[33,34] Similar to the first class of problems, here too, there are several unknown issues. For example, there is hardly any theoretical study that accounts for the pH-dependence of the PEL charge density in calculating the electroosmotic transport in a *soft nanochannel* or the corresponding electrophoretic mobility of soft particles. Similarly, there is hardly any study that provides these electroosmotic velocity and electrophoretic mobility appropriately accounting for the combined equilibrium of the PEL conformation and the EDL electrostatics.

In this paper, we address one of these unaddressed issues related to this second kind of problem. We provide solution for the electroosmotic transport in a polyelectrolyte-grafted nanochannel with pH-dependent charge density. We provide our calculations for the case of a constant PEL thickness. (We discuss the validity of such an assumption in Sec. IV A.) The necessary equilibrium electrostatic calculations are provided in our previous paper.[26] In the present electroosmotic model, the cubic monomeric distribution (resulting from the corresponding electrostatics[26]) impacts the corresponding drag coefficient, which scales as the square of the monomeric concentration distribution. The second important contribution is the explicit consideration of the hydrogen and hydroxyl ions, along with the electrolyte ions, in dictating the net charge density that interacts with the applied electric field to trigger the driving electroosmotic body force. The central result of this paper is that the electroosmotic velocity is substantially weaker for the case of the PEL systems with pH-dependent charge density. Degree of this lowering is of course a function of the parameters, and the corresponding variation exhibits richer behavior for those parameters that affect both the monomer distribution as well as the PEL-EDL electrostatics. We further demonstrate that such unique electroosmotic behavior can be extremely significant in suppressing the electroosmotic flow strength in polyelectrolyte-grafted nanochannels. Such suppression is well beyond the extent typically witnessed in standard polyelectrolyte/polymer-grafted or polyelectrolyte/polymer-adsorbed capillaries,[35–39] and therefore can have large impact in nanochannel electrophoresis based applications such as ion separation,[40,41] DNA elongation,[42] DNA sequencing,[43] and many more.

II. THEORY

We consider a polyelectrolyte-grafted nanochannel of height $2h$, as shown in Fig. 1. The PEL is of thickness d, and its charge is a function of the local hydrogen ion concentration. This stems from the fact that the charging of the PEL occurs by the (weak) acid or base like dissociation of the chargeable sites within the PEL.[7] Here, we shall develop a model to study the electroosmotic transport in such a nanochannel. For that purpose, we shall first propose the corresponding electrostatics and second use this electrostatics calculation to obtain the corresponding electroosmotic velocity profile. Finally, we shall provide the corresponding analysis for the pH-independent PEL charging and pinpoint the differences with the presently studied pH-dependent case.

A. Electrostatics in the polyelectrolyte-grafted nanochannel with pH-dependent charge density

We have solved this electrostatics problem in our previous study.[26] Here, we provide the key results from this study for the sake of continuity. In this study, we identified that the consideration of explicit hydrogen ion concentration is mandatory to describe the EDL electrostatics of polyelectrolyte-grafted nanochannel with pH-dependent charge density. More importantly, we discovered that such a consideration forbade the use of uniform monomer distribution within the PEL. Such uniformity leads to discontinuities in the value and in the gradient of the hydrogen ion concentration at the PEL-electrolyte interface (i.e., at $y=-h+d$ or $y=h-d$ in Fig. 1). These issues get addressed when one considers a *non-unique, cubic* distribution of the monomers within the PEL. Such a distribution not only ensures the continuities in the value and the gradient of the hydrogen ion concentration at the PEL-electrolyte interface but also enforces zero hydrogen flux at the PEL-rigid-solid interface. For the detailed free energy procedure, kindly refer to our previous paper.[26] Here, we start from the modified Poisson equation, describing the EDL electrostatic potential (ψ), which results from this free energy minimization (we consider only the bottom half of the nanochannel)

$$\begin{aligned}\frac{d^2\psi}{dy^2} &= \frac{e}{\varepsilon_0\varepsilon_r}[n_- - n_+ + n_{OH^-} - n_{H^+} + \varphi(y)n_{A^-}] \quad \text{for} -h \le y \le -h+d,\\ \frac{d^2\psi}{dy^2} &= \frac{e}{\varepsilon_0\varepsilon_r}[n_- - n_+ + n_{OH^-} - n_{H^+}] \quad \text{for} -h+d \le y \le 0.\end{aligned} \tag{1}$$

Here, e is the electronic charge, ε_0 is the permittivity of free space, ε_r is the relative permittivity of the medium (assumed identical for the media both inside and outside the PEL[44]), n_i is the number density (having units of $1/m^3$) of the electrolyte ions ($i = \pm, H^+, OH^-$), n_{A^-} is the number density of the PEL ions, and $\varphi(y)$ is the cubic monomer distribution. Here, we assume that both the electrolyte ions as well as the PEL ions are monovalent. We further assume that the PEL ions are negatively charged, which are produced by a weak acid-like dissociation of the polyelectrolyte chargeable sites (*PCS*).[7]

For the evaluation of ψ, we need to obtain the expression for n_i, n_{A^-}, and $\varphi(y)$. Using the same free energy model (see Ref. 26), we get the Boltzmann distribution relating $n_\pm$ and n_{OH^-} to ψ as

$$n_\pm = (n_{\pm,\infty})\exp\left(\mp\frac{e\psi}{k_BT}\right) \quad \text{for } -h \le y \le 0, \tag{2}$$

$$n_{OH^-} = (n_{OH^-,\infty})\exp\left(\frac{e\psi}{k_BT}\right) \quad \text{for } -h \le y \le 0\,. \tag{3}$$

Here, k_BT is the thermal energy and $n_{\pm,\infty}$ and $n_{OH^-,\infty}$ are the bulk number densities of the electrolyte and hydroxyl ions. Again, the same free energy model provides the relationship between n_{OH^+} and ψ

$$\begin{aligned} n_{H^+} &= (n_{H^+,\infty})\exp\left[-\frac{e\psi}{k_BT}\left(1+\varphi(y)\frac{K'_a\gamma}{(K'_a+n_{H^+})^2}\right)\right] \quad \text{for } -h \le y \le -h+d \\ n_{H^+} &= (n_{H^+,\infty})\exp\left(-\frac{e\psi}{k_BT}\right) \quad \text{for } -h+d \le y \le 0 \end{aligned}, \tag{4}$$

where $n_{OH^+,\infty}$ is the bulk number densities of the hydrogen ions, γ is the maximum number density of the *PCS*, and $K'_a = 10^3 N_A K_a$ [N_A is the Avogadro number, K_a (having units of moles/liter) is the ionization constant of the acid *HA* dissociating to produce A^- ions (or PEL ions)]. To obtain n_{A^-}, we employ the condition (see Ref. 7 for details)

$$n_{A^-} = \frac{K'_a\gamma}{K'_a + n_{H^+}}. \tag{5}$$

Please note that the above set of equations is valid for both the cases of overlapping and nonoverlapping EDL thicknesses (see below for the definition of the EDL thickness). This stems from the fact that the bulk concentrations ($n_{\pm,\infty}, n_{OH^-,\infty}, n_{H^+,\infty}$) are not the channel centerline concentrations; rather, they are the concentrations of these ion species at the reservoirs that connect these soft nanochannels. We consider the electrostatic potential at these reservoirs to be zero. This idea was first developed by Baldesaari and Santiago[45] and was later used by us for other studies that considered overlapping cases of overlapped EDLs.[46,47]

Finally, the *cubic distribution* of the monomers is expressed as (with $\bar{y} = y/h$, $\bar{d} = d/h$)

$$\varphi(\bar{y}) = \beta\left(\bar{y}+1-\bar{d}\right)^2\left(\bar{y}+1+\frac{\bar{d}}{2}\right). \tag{6}$$

Selection of the *prefactor* β is discussed later. Under the above conditions, we solve for potential ψ in the presence of the boundary conditions

$$\begin{aligned} &\left(\frac{d\psi}{dy}\right)_{y=-h} = 0; \quad \left(\frac{d\psi}{dy}\right)_{y=0} = 0; \\ &(\psi)_{y=(-h+d)^+} = (\psi)_{y=(-h+d)^-}; \quad \left(\frac{d\psi}{dy}\right)_{y=(-h+d)^+} = \left(\frac{d\psi}{dy}\right)_{y=(-h+d)^-}. \end{aligned} \tag{7}$$

While such boundary conditions ensure continuity in the value and in the gradient of ψ at the PEL-electrolyte interface, consideration of the *cubic* $\varphi(\bar{y})$ in the form expressed in Eq. (6) ensures continuity in the value and the gradient in the hydrogen ion concentration [related to ψ through Eq. (4)]. In fact, the condition expressed in Eq. (6) also ensures no flux condition at the PEL-rigid-solid interface as well as satisfy the constraint $\frac{\sigma}{a^3}\int_{-h}^{-h+d}\varphi(y)dy = N_p$. Here N_p is the number of chargeable sites in a polyelectrolyte molecules, a is the thickness of the chain, and σ is the area of a single polyelectrolyte chain. The parameter β, which dictates the distribution φ of the chargeable site, can be related to the system parameter(s) by using the constraint $\frac{\sigma}{a^3}\int_{-h}^{-h+d}\varphi(y)dy = N_p$. Using Eq. (6) to express φ, we obtain $\beta = \left(\frac{N_p a^3}{d\sigma}\right)\left(\frac{4}{d^3}\right)$ needs to be selected in such a manner that the effect of the PEL ions equivalent for both pH-dependent and pH-independent cases. Now in order to ensure that the total number of chargeable sites remains identical for both the pH-dependent and the pH-independent cases, we enforce $\frac{1}{d}\int_{-h}^{-h+d}\varphi(y)dy = 1$, which in presence of

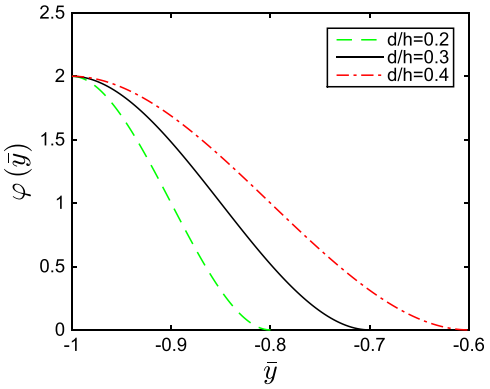

FIG. 2. Variation of $\varphi(\bar{y})$ with $\bar{y}$ for different values of $\bar{d} = d/h$.

the constraint $\frac{\sigma}{a^3}\int_{-h}^{-h+d}\varphi(y)dy = N_p$, will imply $\frac{N_p a^3}{\sigma d} = 1$ and $\beta = \frac{4}{\bar{d}^3}$. β was obtained in the same manner in our previous study.[26] In Fig. 2, we show the variation of $\varphi(\bar{y})$ with $\bar{y}$ for different values of $\bar{d}$. This result will be used later when we discuss the variation of the electroosmotic velocity as a function of different parameters.

It is worthwhile to note here that in addition to the dimensionless parameter β, the electrostatic potential distribution is dictated by three other dimensionless parameters, namely, $\bar{K'}_a = \frac{K'_a}{n_\infty}$, $\bar{\lambda} = \frac{\lambda}{h}$ (where $\lambda = \sqrt{\frac{\varepsilon_0\varepsilon_r k_B T}{2n_\infty e^2}}$ is the EDL thickness), and $K_\lambda = \frac{\lambda_{PEL}}{\lambda} = \sqrt{\frac{2n_\infty}{\gamma}}$ (where $\lambda_{PEL} = \sqrt{\frac{\varepsilon_0\varepsilon_r k_B T}{\gamma e^2}}$ is an equivalent EDL thickness inside the PEL[6,48]). These parameters appear from the appropriate non-dimensionalization of the problem. For this non-dimensionalization procedure (which expresses the equations in terms of the dimensionless potential $\bar{\psi} = e\psi/k_B T$), and the procedure for solving the resulting dimensionless equation(s), kindly refer to our previous paper (see Ref. 26).

B. Electroosmotic transport in the polyelectrolyte-grafted nanochannel with pH-dependent charge density

We consider a steady-state, one dimensional, fully developed axial electroosmotic transport in presence of an externally applied axial electric field E in such a polyelectrolyte-grafted nanochannel with pH-dependent charge density. The equation governing the velocity field u is given by

$$\begin{aligned}\eta\frac{d^2u}{dy^2} + e(n_+ - n_- + n_{H^+} - n_{OH^-})E - \mu_c u = 0 \quad -h \le y \le -h+d,\\ \eta\frac{d^2u}{dy^2} + e(n_+ - n_- + n_{H^+} - n_{OH^-})E = 0 \quad -h+d \le y \le 0,\end{aligned} \tag{8}$$

where η is the dynamic viscosity of the liquid and $\mu_c = \left(\frac{\varphi(y)}{b}\right)^2$ (see Refs. 5 and 49) is the drag coefficient within the PEL (b is the effective monomer size[5]). Please note that following the works of Freed and Edwards[50] and de Gennes,[51] this drag coefficient can be interpreted in terms of the length that screens the background from the flow inside the polymer coil in semi-dilute solution. For the special case, where the flow velocity is much larger than the polymer average velocity, one can express the drag coefficient μ_c as $\mu_c \sim K^2$, where K^{-1} is the screening length. This case specially suits the present problem, where the polymer molecules being grafted to the nanochannel walls are static. Following Ref. 52, we can express $K^{-1} \sim \varphi^{-1}$, so that $\mu_c \sim \varphi^2$. Consideration of the pH dependent charge density explicitly accounting for the hydrogen ion concentration, leads to specific contribution in the description of the electroosmotic velocity. First is the consideration of hydrogen and hydroxyl ions in the description of the mobile ions that interacts with the applied electric field to decide the electroosmotic body force. Once the electrostatic potential field is known, number density of each of these ions can be obtained, as illustrated in Sec. II A. Second, the drag coefficient μ_c will now exhibit a specific variation with y, given the cubic nature of the function $\varphi(y)$ [see Eq. (6) and Fig. 2].

Employing Eqs. (3) and (4), we can express Eq. (8) in dimensionless form as

$$\begin{aligned}&\frac{d^2\bar{u}}{d\bar{y}^2} + \frac{\bar{E}}{\bar{\lambda}^2}\left[-\sinh(\bar{\psi}) - \frac{1}{2}\bar{n}_{OH^-,\infty}\exp(\bar{\psi}) + \frac{1}{2}\bar{n}_{H^+}\right] - \bar{\alpha}^2\varphi^2(\bar{y})\bar{u} = 0 \quad -1 \le \bar{y} \le -1+\bar{d},\\ &\frac{d^2\bar{u}}{d\bar{y}^2} + \frac{\bar{E}}{\bar{\lambda}^2}\left[-\sinh(\bar{\psi}) - \frac{1}{2}\bar{n}_{OH^-,\infty}\exp(\bar{\psi}) + \frac{1}{2}\bar{n}_{H^+,\infty}\exp(-\bar{\psi})\right] = 0 \quad -1+\bar{d} \le \bar{y} \le 0.\end{aligned} \tag{9}$$

In Eq. (9), $\bar{y} = y/h$, $\bar{d} = d/h$, $\bar{\lambda} = \lambda/h$, $\bar{\psi} = e\psi/k_B T$, $\bar{n}_{OH^-,\infty} = \frac{n_{OH^-,\infty}}{n_\infty}$, $\bar{n}_{H^+,\infty} = \frac{n_{H^+,\infty}}{n_\infty}$, $\bar{u} = \frac{u}{u_0}$ (where $u_0 = \frac{k_B T}{e}\frac{\varepsilon_0\varepsilon_r E_0}{\eta}$ is the electroosmotic velocity scale; E_0 is the scale of the electric field), $\bar{E} = \frac{E}{E_0}$, and $\bar{\alpha} = \frac{h}{b\sqrt{\eta}}$. $\bar{u}$ will be obtained by solving Eq. (9) numerically in presence of the conditions

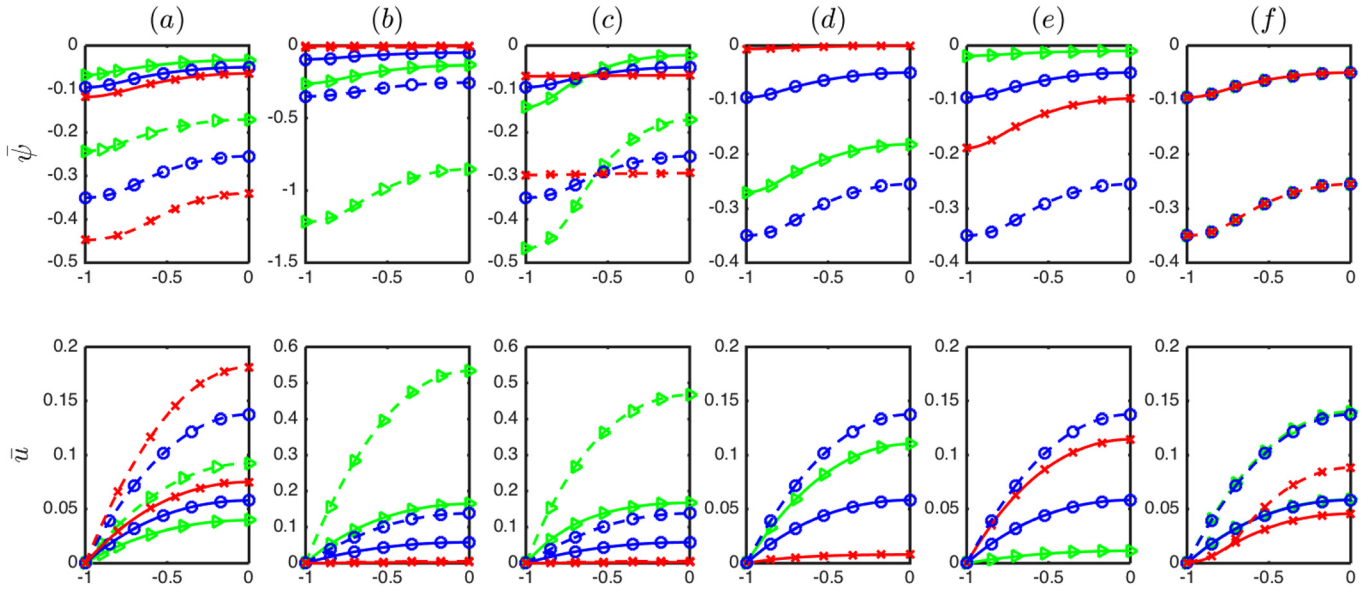

FIG. 3. Transverse variation of the dimensionless electrostatic potential (top panel) and the dimensionless electroosmotic velocity profile (bottom panel). The electrostatic potential is governed by the dimensionless parameters $\bar{d}, K_\lambda, \bar{\lambda}, \bar{n}_{H^+,\infty}$, and $\bar{K}_a^{'}$, while the velocity field is dictated by these same set of parameters as well the additional dimensionless parameter $\bar{\alpha} = \frac{h}{b\sqrt{\eta}}$. For all the figures, we maintain five parameters ($K_\lambda, \bar{\lambda}, \bar{n}_{H^+,\infty}, \bar{K}_a^{'}$, and $\bar{\alpha}$) equal to unity and $\bar{d} = 0.3$, except for (a) $\bar{d} = 0.2$ (triangular markers), $\bar{d} = 0.3$ (circular markers), $\bar{d} = 0.4$ (cross markers), (b) $K_\lambda = 0.5$ (triangular markers), $K_\lambda = 1$ (circular markers), $K_\lambda = 5$ (cross markers), (c) $\bar{\lambda} = 0.5$ (triangular markers), $\bar{\lambda} = 1$ (circular markers), $\bar{\lambda} = 5$ (cross markers), (d) $\bar{n}_{H^+,\infty} = 0.1$ (triangular markers), $\bar{n}_{H^+,\infty} = 1$ (circular markers), $\bar{n}_{H^+,\infty} = 10$ (cross markers), (e) $\bar{K}_a^{'} = 0.1$ (triangular markers), $\bar{K}_a^{'} = 1$ (circular markers), $\bar{K}_a^{'} = 10$ (cross markers), and (f) $\bar{\alpha} = 0.1$ (triangular markers), $\bar{\alpha} = 1$ (circular markers), $\bar{\alpha} = 10$ (cross markers). In (f), we show that $\bar{\alpha}$ affects only $\bar{u}$ and not $\bar{\psi}$. Throughout, we use $\bar{n}_{OH^-,\infty} = \bar{n}_{H^+,\infty}$, and $\bar{E} = 1$. For all the figures, the solid lines represent the case with pH effect, whereas the dashed lines represent the case without pH effects.

$$\left(\frac{d\bar{u}}{d\bar{y}}\right)_{y=-1} = 0; \quad \left(\frac{d\bar{u}}{d\bar{y}}\right)_{y=0} = 0;$$
$$(\bar{u})_{\bar{y}=(-1+d)^+} = (\bar{u})_{\bar{y}=(-1+\bar{d})^-}; \tag{10}$$
$$\left(\frac{d\bar{u}}{d\bar{y}}\right)_{\bar{y}=(-1+\bar{d})^+} = \left(\frac{d\bar{u}}{d\bar{y}}\right)_{y=(-1+\bar{d})^-}.$$

C. Electroosmotic transport in the polyelectrolyte-grafted nanochannel with pH-independent or constant charge density

This is the limiting case of the above formulation. Such pH-independence leads to several simplifications, and the resulting equations have been already derived and solved in the several previous studies including those by the present author(s).[6,44,53,54] Here, we briefly discuss these simplified governing equations, since in the Sec. III we shall compare this case with the electroosmotic transport in polyelectrolyte-grafted nanochannels.

When the charge density of the grafted polyelectrolytes is independent of the pH, the number density of the polyelectrolyte ions is constant, and the corresponding potential distribution (ignoring the explicit hydrogen and hydroxyl ion distribution) can be expressed as

$$\frac{d^2\psi}{dy^2} = \frac{e}{\varepsilon_0\varepsilon_r}[n_- - n_+ + n_{A^-}] \quad \text{for} - h \le y \le -h + d,$$
$$\frac{d^2\psi}{dy^2} = \frac{e}{\varepsilon_0\varepsilon_r}[n_- - n_+] \quad \text{for} - h + d \le y \le 0. \tag{11}$$

Here too, Eq. (2) dictates $n_\pm$, while $n_{A^-} = constant$. Please note that Eq. (11) is effectively derived from the simplified version of the free energy formulation, discussed in our previous paper.[26] ψ can be obtained by solving Eq. (11) in presence of the boundary conditions expressed in Eq. (7). An analytical solution of ψ becomes possible for weak values of the electrostatic potential which allows the employment of the Debye-Hückel linearization;[6] however, for larger values of the potential, a numerical solution is mandatory.[53,54]

Finally, for this simplified case, the velocity field is expressed as

$$\eta\frac{d^2u}{dy^2} + e(n_+ - n_-)E - \frac{1}{b^2}u = 0 \quad -h \le y \le -h + d,$$
$$\eta\frac{d^2u}{dy^2} + e(n_+ - n_-)E = 0 \quad -h + d \le y \le 0. \tag{12}$$

The corresponding dimensionless form is

$$\frac{d^2\bar{u}}{d\bar{y}^2} - \frac{\bar{E}}{\bar{\lambda}^2}\sinh(\bar{\psi}) - \bar{\alpha}^2\bar{u} = 0 \quad -1 \le \bar{y} \le -1 + \bar{d},$$
$$\frac{d^2\bar{u}}{d\bar{y}^2} - \frac{\bar{E}}{\bar{\lambda}^2}\sinh(\bar{\psi}) = 0 \quad -1 + \bar{d} \le \bar{y} \le 0, \tag{13}$$

$\bar{u}$ for this pH-independent case will be obtained by solving Eq. (13) in presence of the Boundary Conditions expressed in Eq. (10).

III. RESULTS

Fig. 3 is the central finding of this paper. Here, we analyze the transverse variation of the electrostatic potential and the electroosmotic velocity as a function of the different parameters dictating the problem. Of course, in our previous paper,[26]

we have discussed these aspects of the electrostatic potential; here, we repeat some of these discussions in order to better explain the corresponding variation of the electroosmotic velocity profiles. Fig. 3(a) provides the transverse variation of the electrostatic potential ($\bar{\psi}$) and the electroosmotic velocity ($\bar{u}$) for different values of the dimensionless PEL thickness $\bar{d}$. Increase in $\bar{d}$ increases the total amount of the PEL charge. This typically leads to an enhanced value of the electrostatic potential at the PEL-rigid-solid interface,[6] thereby causing an enhanced magnitude of the electrostatic potential at any transverse location. This $\bar{d}$-dependent enhancement of the electrostatic potential is similar for pH-independent and pH-dependent charge densities, although the extent of difference for different $\bar{d}$ is more pronounced for the pH-independent case. The corresponding electroosmotic velocity profile [see Fig. 3(a) bottom] is dictated by this particular $\bar{d}$-dependent variation of the electrostatic potential and also the fact that the drag coefficient varies as φ^2 for the pH-dependent case. Of course for the pH-independent case, where the drag coefficient is constant (see Sec. II C), the $\bar{d}$-dependence of the electroosmotic transport is solely dictated by the corresponding electrostatic potential variation, thereby enhancing the electroosmotic flow strength with an enhancement of $\bar{d}$. For the pH-dependent case, in addition to being affected by the enhancement of the electrostatic potential, the electroosmotic velocity strength will also be impacted by the corresponding $\bar{d}$-dependent drag force (see Fig. 2 and Sec. II C). Presence of this drag force as well as relatively weaker value of the electrostatic potential implies that for a given $\bar{d}$, electroosmotic flow strength is substantially weaker for the pH-dependent case. On the other hand, the individual contribution of the electrostatic potential in augmenting the flow strength overwhelms the retarding influence of the drag force being dictated by the drag coefficient that varies as φ^2. Consequently, we find that for the pH-dependent case, the enhancement of $\bar{d}$ augments the strength of the electroosmotic transport.

In Fig. 3(b), we demonstrate the effect of the variation of the parameter $\mathrm{K}_\lambda = \lambda_{\mathrm{PEL}}/\lambda$. Smaller values of K_λ or weaker relative value of the PEL-EDL thickness imply a more enhanced relative value of the number density of the PEL ions. Consequently, for both the pH-dependent and the pH-independent cases, we observe a progressive increase in the magnitude of the electrostatic potential with a lowering of K_λ. Of course for the pH-dependent case, the PEL charging being caused by a partial ionization of the *PCS*, for a given K_λ, $|\bar{\psi}|_{\mathrm{pH-dependent}} < |\bar{\psi}|_{\mathrm{pH-independent}}$. Since the variation of K_λ does not influence φ or the drag force, its impact on the variation of the electroosmotic transport is solely dictated by the corresponding variation of ψ. Consequently, we find that for both the pH-dependent and the pH-independent cases, magnitude of the electroosmotic velocity increases with a decrease in K_λ. Further, for a given K_λ, $(u)_{\mathrm{pH-dependent}} < (u)_{\mathrm{pH-independent}}$.

Fig. 3(c) quantifies the effect of the variation of the dimensionless EDL thickness $\bar{\lambda}$. For both the pH-dependent and the pH-independent cases, larger or overlapped values of $\bar{\lambda}$ lead to a more uniform value of $\bar{\psi}$ across the entire channel height. As a consequence for larger $\bar{\lambda}$, the electroosmotic flow strength is substantially reduced. Such an interrelationship can be explained by noting that the electroosmotic transport is triggered by the variation of the electrostatic potential within the EDL; such variation being very weak for the cases with overlapped $\bar{\lambda}$ there is this reduction of the electroosmotic flow strength. Again the effect of partial dissociation of the PCS for the pH-dependent cases ensures weaker magnitudes of the electrostatic potential and the resulting electroosmotic velocity for the pH-dependent cases. EDL thickness signifies the length scale over which the EDL potential may vary from a charged interface. In the present case, this charged interface is the PEL-electrolyte interface. When $\bar{\lambda} = \lambda/h \ll 1$, the potential in the electrolyte side will quickly decay to zero, whereas the potential in the polyelectrolyte side will saturate to the Donnan potential[7,48] in case $\bar{d} \gg \bar{\lambda}$. (Of course in none of the present plots, we study any of these limiting cases.) For the velocity field u, this signifies that the velocity attains the plug-shaped profile over very small spatial distance (in the electrolyte side) from the PEL-electrolyte interface. On the other hand, the velocity on the side of the PEL will attain a profile that matches with the no-slip boundary condition at the wall ($y = -h$) and the plug flow profile (at locations within the electrolyte).

Fig. 3(d) quantifies the effect of variation of $\bar{n}_{H^+,\infty}$. Of course variation in $\bar{n}_{H^+,\infty}$ only affects the electrostatic potential and the electroosmotic velocity for the case with pH-dependent charge density. Weak values of $\bar{n}_{H^+,\infty}$ indicate a condition of depleted hydrogen ions in the medium; this leads to a more enhanced dissociation of the *PCS*. Consequently, for weak $\bar{n}_{H^+,\infty}$, both the electrostatic potential and the electroosmotic velocity get enhanced.

Variation of $\bar{K}'_a$ also affects the electrostatic potential and the electroosmotic velocity only for the case with pH-dependent charge density [see Fig. 3(e)]. Enhanced $\bar{K}'_a$ causes a more pronounced dissociation of the *PCS*, leading to a more enhanced value of the electrostatic potential and the electroosmotic velocity.

Fig. 3(f) shows the effect of variation of the parameter $\bar{\alpha}$. $\bar{\alpha}$ does not affect the electrostatic potential and only affects the electroosmotic velocity. $\bar{\alpha}$ exerts a strictly non-linear influence on the velocity variation. Therefore, for both the pH-dependent and pH-independent cases, there is imperceptible variation in the velocity when $\bar{\alpha}$ increases from 0.1 to 1, whereas the variation in the velocity becomes significantly large as $\bar{\alpha}$ increases from 1 to 10. Such non-linear behavior indicates that for weak to intermediate values of $\bar{\alpha}$, the contribution of the drag force ($\sim\bar{\alpha}^2$) is negligible and the flow is effectively an non-retarded electroosmotic transport. On the contrary, for larger $\bar{\alpha}$ ($\bar{\alpha} \gg 1$), this retardation becomes prominent causing a substantial decrease in the velocity.

IV. DISCUSSIONS

A. Selection of the PEL thickness *d*

In this study, we assume that the PEL thickness d is chosen strictly by the effects associated with the polymer, namely, the entropic elastic effects, or the stretching energy of the chains and the volume exclusion effects, or the effects associated with the steric repulsion between the monomers, dominate other influences. Therefore, d can be expressed as[55]

$$d = N_p\left(\frac{v_0 b_k^2}{6\sigma}\right)^{1/3} = N_p b_k\left[\frac{(1-2\chi)b_k^2}{6\sigma}\right]^{1/3}, \qquad (14)$$

where b_k is the Kuhn length and $v_0 = b_k^3(1-2\chi)$ is the excluded volume parameter. (χ is the Flory Huggins parameter.) Thus, in the present calculation, it is implicitly assumed that the EDL electrostatic effects do not select d; this justifies the consideration of a constant d in the present study as well as other studies on soft interface EDL electrostatics.[44,54,56–58]

B. Disregard of the multi-dimensionality of the variables and the finite ion size effect

In the present problem, the PEL that we consider is in the form of *Polyelectrolyte brushes*. Through the extensive works of Zhulina, Borisov, Milner, and co-workers,[9,10,13,16,59–62] it has been well established that polyelectrolytes in a brush-like conformation can be very well represented to have a 1-D configuration in a direction perpendicular to the grafting surface. Therefore, the monomer distribution of the polyelectrolyte brushes only depends on y and is independent of other directions. As a consequence, the equilibrium distributions of $n_\pm, n_{H^+}, n_{OH^-}$, and ψ are assumed to be one-dimensional (i.e., vary only in y-direction), and so is the resulting electroosmotic velocity u.

In the present model, we have not considered finite ion size effect. Following Ref. 63, it can be shown that the finite ion size becomes important only when $na^3 \sim 1$ [where n is the number density (in units of $1/m^3$) and a is the ion size] anywhere in the nanochannel. Considering Boltzmann distribution for the ions (please note that all types of ions follow Boltzmann distribution everywhere in the nanochannel, except for the hydrogen ions within the PEL), this critical electrostatic potential (corresponding to which finite ion size effect should be accounted for) is $\psi_c = \frac{k_B T}{e}\ln(n_\infty a^3) \Rightarrow \bar{\psi}_c = \frac{e\psi_c}{k_B T} = \ln(n_\infty a^3)$. Using the ion size a as approximately 0.3 nm, we get $(\bar{\psi}_c)_{c_\infty = 100mM} = -6.42, (\bar{\psi}_c)_{c_\infty = 10mM} = -8.72, (\bar{\psi}_c)_{c_\infty = 1mM} = -11.03$, and $(\bar{\psi}_c)_{c_\infty = 100mM} = -13.33$. Here, c_∞ is the bulk concentration in M (mol/l) and the bulk number density n_∞ (in $1/m^3$) is related c_∞ as $n_\infty = 10^3 N_A c_\infty$ (N_A is the Avogadro number). In the present paper, we always consider small enough number density of the PEL ions so that for any combination of other parameters, the dimensionless electrostatic potential (see Fig. 3) is always much smaller than these above-mentioned values. This justifies the neglect of the finite ion size effects in the present case.

C. Significance of the present study in different soft-nanochannel-based applications

Electric-field-driven transport in microchannels and nanochannels have been widely used for applications such as separation of ions and charged biological species, stretching of polymers like DNA, sequencing of DNA, and many more. Virtually, all these applications rely on the electrophoretic transport of the charged species and rely on their different electrophoretic mobilities. Problem occurs when the electroosmotic transport, triggered on account of the interaction of the applied electric with the ion distribution, gets superposed on the electrophoretic transport of the ions. For example, during the electrophoretic separation, the ions get separated from one another on account of their different electrophoretic mobilities. This separation resolution depends on the extent of difference of their electrophoretic mobility. However, when an electroosmotic velocity, which impacts all the different ions equally gets superposed, the impact of the difference in electrophoretic mobility gets reduced, thereby worsening the separation resolution. Therefore, it has been a long-term practice to devise different methods that may suppress the electroomsotic flow strength in systems meant for applications that rely on electrophoretic transport of ions. One such method has been the use of polyelectrolyte or polymer coating on the inner walls of channels and capillaries[35–39]—presence of such coating invariably leads to suppressed electroosmotic transport. Here, we go one step further and try to investigate the impact of such polyelectrolyte grafting in suppressing the electroosmotic transport for the case where the polyelectrolytes demonstrate a pH-dependent ionization and charging. In order to provide a quantitative comparison between the suppression behaviors for the pH-dependent and the pH-independent cases, we compare the electric field driven ion current (i_{ion}) and the electroosmotic current (i_{eos}) for the two cases.

Following Ref. 43, we can write

$$\begin{aligned}(i_{ion})_{pH-dependent} &= eE\left[\int_{-h}^{h}(\mu_+ n_+ + \mu_- n_- + \mu_{H^+} n_{H^+} + \mu_{OH^-} n_{OH^-})dy\right] \\ &= eE\mu_+ n_\infty h\int_{-1}^{1}\left[\exp(-\bar{\psi}) + \frac{\mu_-}{\mu_+}\exp(\bar{\psi}) + \frac{\mu_{H^+}}{\mu_+}\bar{n}_{H^+}\right. \\ &\quad \left. + \frac{\mu_{OH^-}}{\mu_+}\bar{n}_{OH^-,\infty}\exp(\bar{\psi})\right]d\bar{y}, \qquad (15)\end{aligned}$$

$$\begin{aligned}(i_{ion})_{pH-indepenent} &= eE\int_{-h}^{h}(\mu_+ n_+ + \mu_- n_-)dy \\ &= eEn_\infty\mu_+ h\int_{-1}^{1}\left[\exp(-\bar{\psi}) + \frac{\mu_-}{\mu_+}\exp(\bar{\psi})\right]d\bar{y}, \qquad (16)\end{aligned}$$

where μ_i is the electrophoretic mobility of species i ($i = \pm$, H^+, OH^-).

Similarly following Ref. 64, we can write

$$\begin{aligned}(i_{eos})_{pH-dependent} &= e\left[\int_{-h}^{h}u(n_+ - n_- + n_{H^+} - n_{OH^-})dy\right] \\ &= eu_0 n_\infty h\int_{-1}^{1}\bar{u}[-2\sinh(\bar{\psi}) + \bar{n}_{H^+} \\ &\quad - \bar{n}_{OH^-,\infty}\exp(\bar{\psi})]d\bar{y}, \qquad (17)\end{aligned}$$

$$\begin{aligned}(i_{eos})_{pH-independent} &= e\left[\int_{-h}^{h}u(n_+ - n_-)dy\right] \\ &= eu_0 n_\infty h\int_{-1}^{1}\bar{u}[-2\sinh(\bar{\psi})]d\bar{y}. \qquad (18)\end{aligned}$$

Consequently, we may write

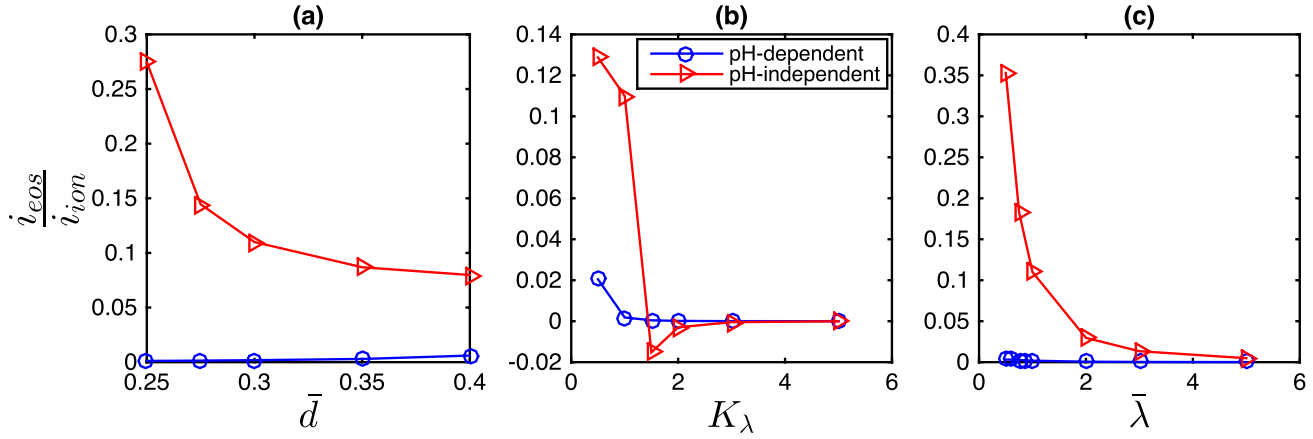

FIG. 4. Variation of the ratio i_{eos}/i_{ion} with (a) $\bar{d}$ ($K_\lambda = 1, \bar{\lambda} = 1$), (b) K_λ ($\bar{d} = 0.3, \bar{\lambda} = 1$), and (c) $\bar{\lambda}$ ($K_\lambda = 1, \bar{d} = 0.3$) for the cases with pH-dependent and pH-independent PEL charge density. For the simulations, we use $\mu_{liq} = 1.76 \times 10^{-8}\text{m}^2/\text{V s}$, $\mu_+ = \mu_{Na^+} = 5 \times 10^{-8}\text{m}^2/\text{V s}$, $\mu_- = \mu_{Cl^-} = -7.9 \times 10^{-8}\text{m}^2/\text{V s}$, $\mu_{H^+} = 36 \times 10^{-8}\text{m}^2/\text{V s}$, and $\mu_{OH^-} = -20 \times 10^{-8}\text{m}^2/\text{V s}$. All other parameters ($\bar{n}_{H^+,\infty}, \bar{K}'_a, \bar{\alpha}, \bar{E}$) are equal to unity.

$$\frac{(i_{eos})_{pH-dependent}}{(i_{ion})_{pH-dependent}} = \frac{\mu_{liq}}{\mu_+}\frac{1}{\bar{E}}\frac{\int_{-1}^{1}\bar{u}\left[-2\sinh(\bar{\psi}) + \bar{n}_{H^+} - \bar{n}_{OH^-,\infty}\exp(\bar{\psi})\right]d\bar{y}}{\int_{-1}^{1}\left[\exp(-\bar{\psi}) + \frac{\mu_-}{\mu_+}\exp(\bar{\psi}) + \frac{\mu_{H^+}}{\mu_+}\bar{n}_{H^+} + \frac{\mu_{OH^-}}{\mu_+}\bar{n}_{OH^-,\infty}\exp(\bar{\psi})\right]d\bar{y}}, \tag{19}$$

$$\frac{(i_{eos})_{pH-independent}}{(i_{ion})_{pH-independent}} = \frac{\mu_{liq}}{\mu_+}\frac{1}{\bar{E}}\frac{\int_{-1}^{1}\bar{u}\left[-2\sinh(\bar{\psi})\right]d\bar{y}}{\int_{-1}^{1}\left[\exp(-\bar{\psi}) + \frac{\mu_-}{\mu_+}\exp(\bar{\psi})\right]d\bar{y}}, \tag{20}$$

where $\mu_{liq} = \frac{k_B T}{e}\frac{\varepsilon_0\varepsilon_r}{\eta}$.

Fig. 4 shows the variation of these two ratios $[\frac{(i_{eos})_{pH-dependent}}{(i_{ion})_{pH-dependent}}$ and $\frac{(i_{eos})_{pH-independent}}{(i_{ion})_{pH-independent}}]$ for the different combination of the dimensionless parameters. It can be easily seen that for majority combinations of the parameters, we invariably get $\frac{(i_{eos})_{pH-dependent}}{(i_{ion})_{pH-dependent}} \ll \frac{(i_{eos})_{pH-independent}}{(i_{ion})_{pH-independent}}$, indicating that the nanochannels with grafted with PELs that exhibit pH-dependent ionization can be extremely good electroosmotic flow suppressor.

V. CONCLUSIONS

In this paper, we provide a new theory to calculate the electroomsotic flow profile in nanochannels grafted with the PELs that exhibit a pH-dependent charge density. The results demonstrate distinctly weakened electroosmotic flow strength, and therefore establish such nanochannels as excellent electroosmotic flow suppressors that can be successfully employed for a myriad of applications relying on electrophoretic transport of ions and charged bio-moieties.

[1]G. W. de Groot, M. G. Santonicola, K. Sugihara, T. Zambelli, E. Reimhult, J. Vörös, and G. J. Vancso, "Switching transport through nanopores with pH-responsive polymer brushes for controlled ion permeability," ACS Appl. Mater. Interfaces **5**, 1400 (2013).
[2]B. Yameen, M. Ali, R. Neumann, W. Ensinger, W. Knoll, and O. Azzaroni, "Single conical nanopores displaying pH-tunable rectifying characteristics. Manipulating ionic transport with zwitterionic polymer brushes," J. Am. Chem. Soc. **131**, 2070 (2009).
[3]M. Ali, B. Yameen, J. Cervera, P. Ramirez, R. Neumann, W. Ensinger, W. Knoll, and O. Azzaroni, "Layer-by-layer assembly of polyelectrolytes into ionic current rectifying solid-state nanopores: Insights from theory and experiment," J. Am. Chem. Soc. **132**, 8338 (2010).
[4]M. Ali, B. Yameen, R. Neumann, W. Ensinger, W. Knoll, and O. Azzaroni, "Biosensing and supramolecular bioconjugation in single conical polymer nanochannels. Facile incorporation of biorecognition elements into nanoconfined geometries," J. Am. Chem. Soc. **130**, 16351 (2008).
[5]S. P. Adiga and D. W. Brenner, "Stimuli-responsive polymer brushes for flow control through nanopores," J. Funct. Biomater. **3**, 239 (2012).
[6]S. Chanda, S. Sinha, and S. Das, "Streaming potential and electroviscous effects in soft nanochannels: Towards designing more efficient nanofluidic electrochemomechanical energy converters," Soft Matter **10**, 7558 (2014).
[7]S. Das, "Explicit interrelationship between Donnan and surface potentials and explicit quantification of capacitance of charged soft interfaces with pH-dependent charge density," Colloid. Surf. A **462**, 69 (2014).
[8]R. Zimmermann, S. S. Dukhin, C. Werner, and J. F. L. Duval, "On the use of electrokinetics for unraveling charging and structure of soft planar polymer films," Curr. Opin. Colloid Interface Sci. **18**, 83 (2013).
[9]S. T. Milner, "Polymer brushes," Science **251**, 905 (1991).
[10]S. T. Milner, T. A. Witten, and M. E. Cates, "Theory of the grafted polymer brush," Macromolecules **21**, 2610 (1988).
[11]M. Tagliazucchi, O. Azzaroni, and I. Szleifer, "Responsive polymers end-tethered in solid-state nanochannels: When nanoconfinement really matters," J. Am. Chem. Soc. **132**, 12404 (2010).
[12]S. A. Egorov, A. Milchev, L. Klushin, and K. Binder, "Structural properties of concave cylindrical brushes interacting with free chains," Soft Matter **7**, 5669 (2011).
[13]E. B. Zhulina and O. V. Borisov, "Structure and interaction of weakly charged polyelectrolyte brushes: Self-consistent field theory," J. Chem. Phys. **107**, 5952 (1997).
[14]F. A. M. Leermakers, M. Ballauff, and O. V. Borisov, "On the mechanism of uptake of globular proteins by polyelectrolyte brushes: A two-gradient self-consistent field analysis," Langmuir **23**, 3937 (2007).
[15]S. J. Miklavic and S. MarEelja, "Interaction of surfaces carrying grafted polyelectrolytes," J. Phys. Chem. **92**, 6718 (1988).
[16]R. Israels, F. A. M. Leermakers, G. J. Fleer, and E. B. Zhulina, "Charged polymeric brushes: Structure and scaling relations," Macromolecules **27**, 3249 (1994).
[17]N. P. Shusharina and P. Linse, "Polyelectrolyte brushes with specific charge distribution: Mean-field lattice theory," Eur. Phys. J. E **4**, 399 (2001).
[18]O. Pizio and S. Sokołowski, "Restricted primitive model for electrolyte solutions in slit-like pores with grafted chains: Microscopic structure,

thermodynamics of adsorption, and electric properties from a density functional approach," J. Chem. Phys. **138**, 204715 (2013).
[19]S. He, H. Merlitz, L. Chen, J.-U. Sommer, and C.-X. Wu, "Polyelectrolyte brushes: MD simulation and SCF theory," Macromolecules **43**, 7845 (2010).
[20]D. J. Sandberg, J.-M. Y. Carrillo, and A. V. Dobrynin, "Molecular dynamics simulations of polyelectrolyte brushes: From single chains to bundles of chains," Langmuir **23**, 12716 (2007).
[21]D. Russano, J.-M. Y. Carrillo, and A. V. Dobrynin, "Interaction between brush layers of bottle-brush polyelectrolytes: Molecular dynamics simulations," Langmuir **27**, 11044 (2011).
[22]J.-M. Y. Carrillo and A. V. Dobrynin, "Morphologies of planar polyelectrolyte brushes in a poor solvent: Molecular dynamics simulations and scaling analysis," Langmuir **25**, 13158 (2009).
[23]H. Ouyang, Z. Xia, and J. Zhe, "Static and dynamic responses of polyelectrolyte brushes under external electric field," Nanotechnology **20**, 195703 (2009).
[24]Q. Cao, C. Zuo, L. Li, and G. Yan, "Effects of chain stiffness and salt concentration on responses of polyelectrolyte brushes under external electric field," Biomicrofluidics **5**, 044119 (2011).
[25]D. I. Dimitrov, A. Milchev, and K. Binder, "Polymer brushes in solvents of variable quality: Molecular dynamics simulations using explicit solvent," J. Chem. Phys. **127**, 084905 (2007).
[26]G. Chen and S. Das, "Electrostatics of soft charged interfaces with pH-dependent charge density: Effect of consideration of appropriate hydrogen ion concentration distribution," RSC Adv. **5**, 4493 (2015).
[27]K. McDaniel, F. Valcius, J. Andrews, and S. Das, "Electrostatic potential distribution of a soft spherical particle with a charged core and pH-dependent charge density," Colloids Surf., B **127**, 143 (2015).
[28]J. F. L. Duval, D. Küttner, M. Nitschke, C. Werner, and R. Zimmermann, "Interrelations between charging, structure and electrokinetics of nanometric polyelectrolyte films," J. Colloid Interface Sci. **362**, 439 (2013).
[29]H. Ohshima, T. W. Healy, and L. R. White, "Approximate analytic expressions for the electrophoretic mobility of spherical colloidal particles and the conductivity of their dilute suspensions," J. Chem. Soc. Faraday Trans. 2 **79**, 1613 (1983).
[30]H. Ohshima, "On the general expression for the electrophoretic mobility of a soft particle," J. Colloid Interface Sci. **228**, 190 (2000).
[31]H. Ohshima, "Electrokinetic phenomena of soft particles," Curr. Opin. Colloid Interface Sci. **18**, 73 (2013).
[32]J. F. L. Duval and H. Ohshima, "Electrophoresis of diffuse soft particles," Langmuir **22**, 3533 (2006).
[33]F. Tessier and G. W. Slater, "Modulation of electroosmotic flow strength with end grafted polymer chains," Macromolecules **39**, 1250 (2006).
[34]Z. Zhang, C. Zuo, Q. Cao, Y. Ma, and S. Chen, "Modulation of electroosmotic flow using polyelectrolyte brushes: A molecular dynamics study," Macromol. Theory Simul. **21**, 145 (2012).
[35]Q. Gao and E. S. Yeung, "A matrix for DNA separation: Genotyping and sequencing using Poly(vinylpyrrolidone) solution in uncoated capillaries," Anal. Chem. **70**, 1382 (1998).
[36]S. Qi, X. Liu, S. Ford, J. Barrows, G. Thomas, K. Kelly, A. McCandless, K. Lian, J. Goettert, and S. A. Soper, "Microfluidic devices fabricated in poly(methyl methacrylate) using hot-embossing with integrated sampling capillary and fiber optics for fluorescence detection," Lab Chip **2**, 88 (2002).
[37]L. Bendahl, S. H. Hansen, and B. Gammelgaard, "Capillaries modified by noncovalent anionic polymer adsorption for capillary zone electrophoresis, micellar electrokinetic capillary chromatography and capillary electrophoresis mass spectrometry," Electrophoresis **22**, 2565 (2001).
[38]B. Pranaityte and A. Padarauskas, "Characterization of the SDS-induced electroosmotic flow in micellar electrokinetic chromatography with cationic polyelectrolyte-coated capillaries," Electrophoresis **27**, 1915 (2006).
[39]Y. Zuo, G. Wang, Y. Yu, C. Zuo, Z. Liu, D. Hu, and Y. Wang, "Suppression of electroosmotic flow by polyampholyte brush," Microfluid. Nanofluid. **17**, 923 (2014).
[40]D. Kaniansky, M. Masar, and J. Bielcıkova, "Electroosmotic flow suppressing additives for capillary zone electrophoresis in a hydrodynamically closed separation system," J. Chromotogr. A **792**, 483 (1997).
[41]T. Kaneta, T. Ueda, K. Hata, and T. Imasaka, "Suppression of electroosmotic flow and its application to determination of electrophoretic mobilities in a poly(vinylpyrrolidone)-coated capillary," J. Chromotogr. A **1106**, 52 (2006).
[42]F. I. Uba, S. R. Pullagurla, N. Sirasunthorn, J. Wu, S. Park, R. Chantiwas, Y.-K. Cho, H. Shin, and S. A. Soper, "Surface charge, electroosmotic flow and DNA extension in chemically modified thermoplastic nanoslits and nanochannels," Analyst **140**, 113 (2015).
[43]S. Das, P. Dubsky, A. van den Berg, and J. C. T. Eijkel, "Concentration polarization in translocation of DNA through nanopores and nanochannels," Phys. Rev. Lett. **108**, 138101 (2012).
[44]H. Ohshima, "Theory of electrostatics and electrokinetics of soft particles," Sci. Technol. Adv. Mater. **10**, 063001 (2009).
[45]F. Baldessari and J. G. Santiago, "Electrokinetics in nanochannels. Part I. Electric double layer overlap and channel-to-well equilibrium," J. Colloid Interface Sci. **325**, 526 (2008).
[46]S. Das, A. Guha, and S. K. Mitra, "Exploring new scaling regimes for streaming potential and electroviscous effects in a nanocapillary with overlapping electric double layers," Anal. Chim. Acta **804**, 159 (2013).
[47]S. Das, S. Chanda, J. C. T. Eijkel, N. R. Tas, S. Chakraborty, and S. K. Mitra, "Filling of charged cylindrical capillaries," Phys. Rev. E **90**, 043011 (2014).
[48]S. Chanda and S. Das, "Effect of finite ion sizes in an electrostatic potential distribution for a charged soft surface in contact with an electrolyte solution," Phys. Rev. E **89**, 012307 (2014).
[49]S. P. Adiga and D. W. Brenner, "Toward designing smart nanovalves: Modeling of flow control through nanopores via the helix-coil transition of grafted polypeptide chains," Macromolecules **40**, 1342 (2007).
[50]K. F. Freed and S. F. Edwards, "Polymer viscosity in concentrated solutions," J. Chem. Phys. **61**, 3626 (1974).
[51]P. G. de Gennes, "Dynamics of entangled polymer solutions. II. Inclusion of hydrodynamic interactions," Macromolecules **9**, 594 (1976).
[52]J. Klein, "Shear of polymer brushes," Colloids Surf., A **86**, 63 (1994).
[53]G. Chen and S. Das, "Streaming potential and electroviscous effects in soft nanochannels beyond Debye-Hückel linearization," J. Colloid Interface Sci. **445**, 357 (2015).
[54]H. Ohshima, "Electrical phenomena in a suspension of soft particles," Soft Matter **8**, 3511 (2012).
[55]E. Tsori, D. Andelman, and J.-F. Joanny, "Interfacial instability of charged–end-group polymer brushes," Eur. Phys. Lett. **82**, 46001 (2008).
[56]K. Makino and H. Ohshima, "Soft particle analysis of electrokinetics of biological cells and their model systems," Sci. Technol. Adv. Mater. **12**, 023001 (2011).
[57]H. Ohshima, "Electrostatic interaction between soft particles," J. Colloid Interface Sci. **328**, 3 (2008).
[58]A. C. Barbati and B. J. Kirby, "Soft diffuse interfaces in electrokinetics—Theory and experiment for transport in charged diffuse layers," Soft Matter **8**, 10598 (2012).
[59]Y. B. Zhulina, V. A. Pryamitsyn, and O. V. Borisov, "Structure and conformational transitions in grafted polymer chain layers. A new theory," Polym. Sci. U.S.S.R. **31**, 205 (1989).
[60]S. T. Milner, "Hydrodynamic penetration into parabolic brushes," Macromolecules **24**, 3704 (1991).
[61]S. T. Milner, "Strongly stretched polymer brushes," J. Polymer Sci.: Part B: Polymer Phys. **32**, 2743 (1994).
[62]S. T. Milner, T. A. Witten, and M. E. Cates, "A parabolic density profile for grafted polymers," Europhys. Lett. **5**, 413 (1988).
[63]M. S. Kilic, M. Z. Bazant, and A. Ajdari, "Steric effects in the dynamics of electrolytes at large applied voltages. I. Double-layer charging," Phys. Rev. E **75**, 021502 (2007).
[64]I. Vlassiouk, S. Smirnov, and Z. Siwy, "Ionic selectivity of single nanochannels," Nano Lett. **8**, 1978 (2008).